J Mater Sci (2009) 44:6090–6099
DOI 10.1007/s10853-009-3840-x

Improvement of photopolymer materials for holographic data storage

Michael R. Gleeson · Shui Liu · John T. Sheridan

Received: 7 July 2009 / Accepted: 21 August 2009 / Published online: 4 September 2009

Abstract Photopolymer materials are practical materials for use as holographic recording media due to the fact that they are inexpensive, self-processing materials with the ability to record low loss, highly diffraction efficient volume holographic gratings. In general these materials absorb light of an appropriate wavelength, causing photo-polymerization of the local monomer, inducing a change in the material's refractive index. These small changes in refractive index enable the storage of large quantities of data using holographic techniques. In an attempt to further develop the data storage capacity and quality of the information stored, i.e., resolution, in such materials, a deeper understanding of the photochemical mechanisms present during the formation of holographic gratings has become ever more crucial. From this understanding the response of an acrylamide/polyvinylalcohol based photopolymer to high spatial frequency information is improved through the addition of a chain transfer agent, i.e., sodium formate, HCOONa.

Introduction

In recent years, free-radical photopolymer materials have received a great deal of attention for many applications such as holographic data storage [1, 2]. Their versatility, ease of use, and self-processing ability give them many advantages over more traditional materials such as silver halide and DCG [3]. While the electromagnetic modelling of scatter by 'thick' volume holograms has received a great deal of attention in the literature [4], the formation of these gratings in free radical photopolymer materials has received significantly less attention.

Much of the work discussed in this paper involves developing a fuller understanding of the formation processes that occur during the optical recording of unslanted volume holographic gratings. In order to further improve the performance of photopolymer materials, for applications such as holographic data storage and embedded photopolymer waveguides, a complete and physically realistic theoretical model of the photochemical processes that occur during photo-polymerization must be developed. A study of the photochemical kinetics involved during holographic recording in an acrylamide/polyvinylalcohol (AA/PVA) based photopolymer material is presented [5–7]. Specifically we aim to increase the understanding of what takes place inside the material during holographic recording. We thus aim to extend the validity of our theoretical model, the Non-Local Photopolymerization Driven Diffusion (NPDD) model, based on this improved understanding.

Recording information holographically in photopolymers, typically involves the material being exposed with a coherent light field, (i.e., from a laser source), containing information which is to be optically stored. The ability of the photopolymer being examined to record this information is what determines its quality as a storage medium. In order to holographically test photopolymers in a reproducible fashion, the material is typically exposed to a simple sinusoidal interference pattern of a suitable wavelength.

M. R. Gleeson (✉) · S. Liu · J. T. Sheridan
School of Electrical, Electronic and Mechanical Engineering, UCD Communications and Optoelectronic Research Centre, SFI Strategic Research Cluster in Solar Energy Conversion, College of Engineering, Mathematical and Physical Sciences, University College Dublin, Belfield, Dublin 4, Republic of Ireland
e-mail: michael.gleeson@ucd.ie

S. Liu
e-mail: shui.liu@ucd.ie

J. T. Sheridan
e-mail: john.sheridan@ucd.ie

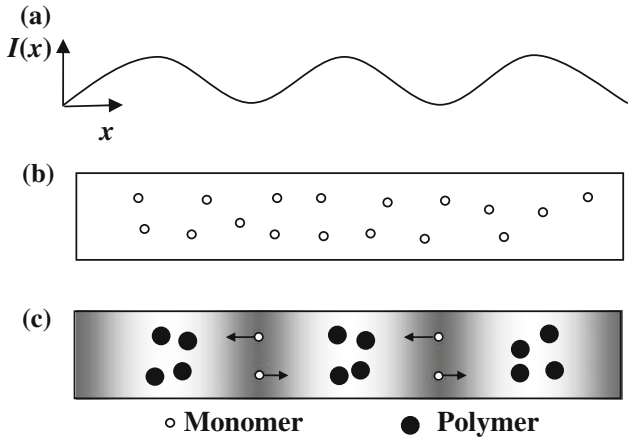

Fig. 1 Grating formation in a photopolymer material: (**a**) illustrates the sinusoidal illuminating intensity distribution at the photopolymer plate; (**b**) represents the photopolymer before recording; and (**c**) represents the photopolymer during recording including monomer diffusion effects

When coherent light interferes, bright and dark fringes are produced as a result of constructive and destructive interference, as in Fig. 1a where $I(x)$ is the exposing irradiance as a function of space. Exposing the photopolymer material, as illustrated in Fig. 1b, to this interference pattern causes polymerization to occur most strongly in the regions of high intensity, i.e., where constructive interference occurs (bright regions). As monomer is consumed in these regions due to polymerization, a monomer concentration gradient is created. The excess monomer in the weakly illuminated regions (dark regions) begins to diffuse into the brighter regions in order to eliminate the concentration gradient, as indicated in Fig. 1c. This results in a sinusoidal polymer concentration distribution. Assuming all the monomer is converted to polymer (which in general has a higher refractive index), a variation of the refractive index of the material will be formed, which is proportional to the polymer concentration distribution.

The NPDD model predicts the high-spatial frequency roll-off, which has been observed experimentally, by assuming spatially non-local chain growth [6–8]. High-spatial frequency roll-off occurs when growing polymer chains propagate into regions where refractive index variations are undesired, i.e., outside the region where the information is being stored, (the dark regions of the interference pattern). This prediction suggests that a reduction in the average polymer chain length, which is grown during photo-polymerization, would reduce the non-locality of the polymer chains, and hence improve the spatial frequency response of a given photopolymer material, i.e., keeping polymer chain growth localized to the bright regions of the exposure. Specifically we aim to achieve this reduction in non-local chain growth with the introduction of a chain transfer agent (CTA), sodium formate.

In order to systematically present the result of this study, the paper is structured as follows: In "Photochemical processes" section, we first discuss the photochemical reactions, which determine the mechanisms present during grating formation. A flow chart of these processes is presented, which succinctly summarizes these photochemical reactions. In "Model development" section, we further develop the theoretical NPDD model to incorporate the photochemical mechanisms presented in "Photochemical processes" section. Then simulations of the behavior of the monomer, polymer, and refractive index changes within the material are presented to illustrate the photochemical reactions, which occur during holographic grating formation. In "Experimental examination" section, we briefly review the experimental preparation of the photopolymer samples, (with and without CTA present), and the experimental techniques used to optically test the performance of these materials. In "Model predictions" section, the extended NPDD model is fit to experimental data using a numerical least squares fitting algorithm in order to compare the performance of the two materials under examination, i.e.,: (a) The standard AA/PVA photopolymer; and (b) the AA/PVA photopolymer with CTA. Estimations of the parameter values associated with the photochemical reactions are then extracted using a fitting algorithm and the results are presented and discussed. Finally a brief conclusion is given.

Photochemical processes

Review of kinetic models

Many of the models presented in the literature involve the assumption of a pseudo-steady state approximation for macroradical concentration [9]. They operate by setting the rate of generation of radicals through photo-initiation, equal to the rate of bimolecular termination. This results in the polymerization rate (R_p) being given by the expression

$$R_p = k_p[M^\bullet][M] = k_p\sqrt{\phi R_i/k_t}[M] \quad (1)$$

where k_p and k_t are the kinetic constants of propagation and termination, respectively, R_i is the rate of decomposition of the initiator species, ϕ is the initiator efficiency and M and $M^\bullet$ are the instantaneous concentrations of monomer and of all macroradicals, respectively. The term macroradical refers to all growing polymer chains, i.e., $n > 0$ monomer units that have an active tip [10].

When a photopolymer material with a low initiator concentration is exposed to a moderate intensity, the linear dependence between polymerization rate, the monomer concentration, and the square root dependence on the rate

of initiation, has been found to agree quite well with experimentally determined rates [5, 11]. In this case, the concentration of primary or initiator radicals, $R^{\bullet}$, (radicals derived directly from photo-cleavage of the initiator molecule), is very low, and as a result macroradicals, $M_n^{\bullet}$ [7, 10, 12], are much more likely to undergo termination involving another macroradical, i.e., *bimolecular termination* (chain–chain), rather than termination with a primary radical i.e., *primary termination* (chain–primary radical). Under these conditions, the steady state assumption is valid and Eq. 1 describes the polymerization kinetics well.

However, studies have shown [13–15], that at high initiation rates, the dependence on initiation drops below that predicted by the square root dependence in Eq. 1. In this case, the steady state assumption is violated and the deviation from the ideal kinetic behavior described by Eq. 1 becomes pronounced. These effects have been attributed to a phenomenon known as primary radical termination, i.e., *primary termination*, [13–15]. At these higher initiation rates, there is a significantly larger primary radical concentration, which, as a result, increases the likelihood of primary termination. Furthermore, since the primary radicals can act to limit the build-up of macroradicals, they can effectively reduce the increase in the polymerization rate that is normally seen during autoacceleration [10].

To proceed, we begin by presenting a consistent set of chemical reaction equations, which allow us to: (i) remove the steady state approximation for macroradical concentration; (ii) include spatially and temporally non-local polymer chain growth; (iii) include time varying photon absorption; (iv) simultaneously include the effects of both primary, i.e., $R^{\bullet}$–$M^{\bullet}$, and bimolecular, i.e., $M^{\bullet}$–$M^{\bullet}$, termination; and (v) include polymerization inhibiting effects.

Reaction mechanisms

The kinetic model presented in this analysis is based upon the following four reaction processes,

I. Initiation

$$I \xrightarrow{h\nu} 2R^{\bullet}, \tag{2a}$$

$$R^{\bullet} + M \xrightarrow{k_i} M_1^{\bullet} = \text{Chain Initiator}. \tag{2b}$$

II. Propagation

$$M_n^{\bullet} + M \xrightarrow{k_p} M_{n+1}^{\bullet} = \text{Growing Polymer Chain}. \tag{3}$$

III. Termination

$$M_n^{\bullet} + M_m^{\bullet} \xrightarrow{k_{tc}} M_{n+m} = \text{Dead Polymer}, \tag{4a}$$

$$M_n^{\bullet} + M_m^{\bullet} \xrightarrow{k_{td}} M_n + M_m = \text{Dead Polymer}, \tag{4b}$$

$$M_n^{\bullet} + R^{\bullet} \xrightarrow{k_{tp}} M_n R = \text{Dead Polymer}. \tag{4c}$$

IV. Inhibition

$$R^{\bullet} + Z \xrightarrow{k_{z,R^{\bullet}}} (R + Z^{\bullet}, \text{ and/or } RZ^{\bullet}) = \text{Scavenged Radical}. \tag{5a}$$

$$M_n^{\bullet} + Z \xrightarrow{k_{z,M^{\bullet}}} (M_n + Z^{\bullet}, \text{ and/or } M_n Z^{\bullet}) = \text{Dead Polymer}. \tag{5b}$$

In the above set of chemical equations, I is the initiator concentration, $h\nu$ indicates the energy absorbed from a photon, M is the monomer concentration, Z is the inhibitor concentration, M_n, M_m, M_{n+m}, M_nR, and $M_nZ^{\bullet}$ represent polymer species with no active propagating tip, i.e., *Dead Polymer*. The term *Dead Polymer* signifies the cessation of the growth of a propagating macroradical of n monomer units, [10], while the term *Scavenged Radical* signifies the removal of a primary radical, [10, 11, 16–18].

Initiation

The initiation process involves two steps: The first step is the production of free radicals, Eq. 2a. This occurs when dye molecules are exposed to light of a suitable wavelength, they absorb photons of light and are promoted to their excited states. These excited states then react with the electron donor to produce a pair of radicals, $R^{\bullet}$. If we consider a grating formed by the interference of two plane waves, the spatial distribution of irradiance is co-sinusoidal, (see Fig. 1), [4–9, 11, 12], and the governing Eq. 2a, for the rate of primary radical production can be given as

$$R_i(x,t) = R_i(t)[1 + V\cos(Kx)] = 2\Phi I_a(t)[1 + V\cos(Kx)], \tag{6}$$

where Φ is the number of primary radicals produced per photon absorbed, the inclusion of the factor of two follows the convention that indicates that two primary radicals are produced for every photon absorbed, [10, 19], V is the fringe visibility, $K = 2\pi/\Lambda$, the grating vector magnitude, and Λ is the grating period. The time varying absorbed intensity, $I_a(t)$ (Einstein/cm^3 s), is given by an adaptation of the Lambert–Beer equation,

$$I_a(t) = \frac{I_0'}{d}\left\{\frac{[\exp(\varepsilon d A_0) - 1]\exp(-\varepsilon\phi I_0' t)}{1 + [\exp(\varepsilon d A_0) - 1]\exp(-\varepsilon\phi I_0' t)}\right\}, \tag{7}$$

where d (cm) is the layer thickness, A_0 (mol/cm^3) is the initial photosensitizer concentration, ϕ (mol/Einstein) is the quantum yield, and ε (cm^2/mol) is the molar absorption

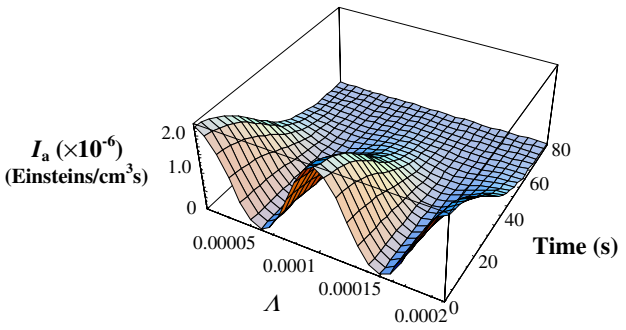

Fig. 2 Plot of the time varying absorbed intensity in Einsteins/cm^{3}s across a period of exposure for a material layer of thickness $d = 110$ μm

coefficient. $I_0' = I_i\left(\frac{\lambda}{N_a hc}\right)T_{sf}$ (Einstein/cm^{2}s) is the exposure intensity, where I_i (mW/cm^{2}s) is the incident intensity, $N_a = 6.02 \times 10^{23}$ mol^{-1} is Avogadro's constant, $c = 3 \times 10^8$ ms^{-1} is the speed of light, $h = 6.62 \times 10^{-34}$ Js is Plank's constant, and T_{sf} is an experimentally estimated loss parameter, which takes into account Fresnel and scattered losses. A simple simulation of the variation of absorbed intensity in time and space can be observed in Fig. 2 where it is assumed that $\varepsilon = 2 \times 10^8$ cm^2/mol, $\phi = 0.021$ mol/Einstein, $d = 110$ μm, and $T_{sf} = 0.74$ [18, 19].

The second step, in the initiation process is chain initiation, Eq. 2b, in which the primary radicals produced due to the absorption of photons react with the monomer to produce the chain initiating species $M_1^{\bullet}$, [10]. The kinetic rate constant for this step is k_i (cm^3 mol^{-1} s^{-1}), i.e., the chain initiation kinetic constant.

Propagation

The propagation step described in Eq. 3 shows a monomer being added to a growing macroradical chain of n repeat monomeric units, where the propagation rate kinetic constant is denoted by k_p (cm^3 mol^{-1} s^{-1}), see the flow chart in Fig. 3.

Termination

In Eqs. 4a–4c three possible termination reactions are presented. Equations 4a and 4b represent the bimolecular termination mechanisms, where two growing macroradicals come together and terminate. This method of termination can occur by either combination (k_{tc}), Eq. 4a, or by disproportionation (k_{td}), Eq. 4b. Since the specific mode of termination does not effect the polymerization kinetics both will be treated in this analysis using a single lumped rate constant, $k_t = k_{tc} + k_{td}$, (cm^3 mol^{-1} s^{-1}), see Fig. 3.

Equation 4c presents the third possible termination mechanism, primary radical termination. In this step, a

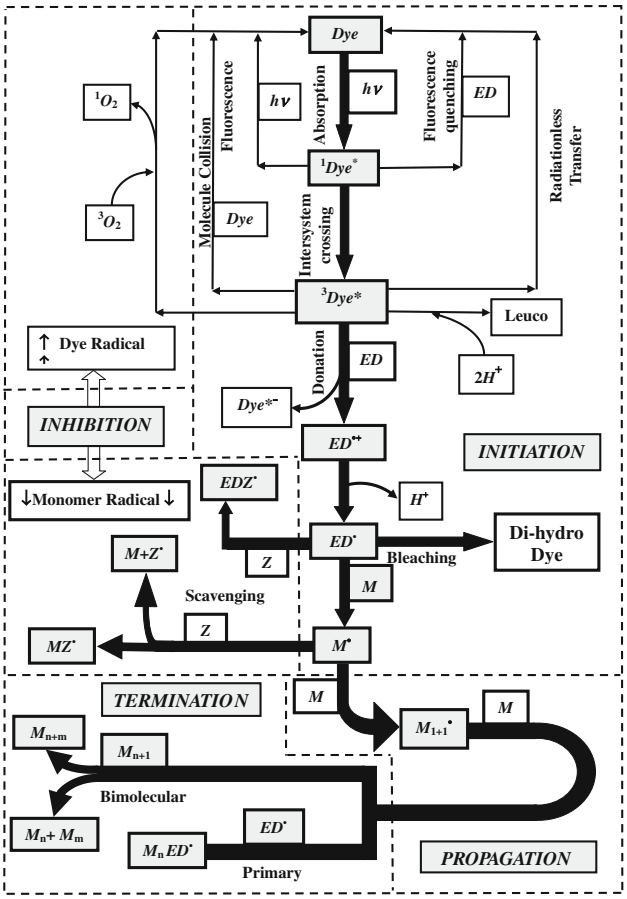

Fig. 3 Flow chart of the major photochemical reactions, which occur during holographic grating formation in photopolymer materials

growing macroradical reacts with a primary radical to form an inactive polymer chain or *Dead Polymer*. The kinetic rate constant for this step will in general be different to that for the bimolecular termination step for two main reasons: (a) the reactivity of the primary radical can be very different to that of the chain end radical, (radical reactivity can depend on molecular size [10]); and (b) the primary radicals will be much more mobile as they are much smaller than the growing macroradicals and therefore the diffusion controlled effects, (caused by viscosity changes due to polymerization), of the two reactions will be quite different. In the analysis presented here the effects of primary radical recombination will be neglected as it has been shown that these events are negligible when compared to other polymerization kinetic reaction, [13, 20].

Inhibition

The final reaction mechanism, presented in Eqs. 5a and 5b, is inhibition caused by the reaction of the primary radicals and macroradicals with inhibitors, such as initially dissolved oxygen in the photopolymer material, [7, 10, 11, 16–18]. These radical-consuming reactions tend to:

(i) suppress the creation of macroradicals by scavenging primary radicals, Eq. 5a; and/or (ii) to inhibit the macroradicals that are created, Eq. 5b.

This process therefore acts to stop the production of polymer chains and most obviously causes an inhibition or dead-band period at the start of grating growth. This inhibition period will continue until there is a sufficiently low concentration of inhibitor in the material to allow polymerization to occur, [7, 10, 11, 16–18]. The kinetics presented in Eqs. 5a and 5b, are simplified by assuming that $Z^{\bullet}$, $MZ^{\bullet}$, and $RZ^{\bullet}$ do not reinitiate polymerization and also that they terminate without regeneration, i.e., they are removed from any possible future reactions.

In order to succinctly summarize all of the major photochemical processes discussed in this section, a flow chart is presented in Fig. 3.

Model development

Based on the analysis of the photochemical mechanisms presented in "Photochemical processes" section, we now combine these reactions into the associated coupled differential equations in both time and space for the main components of the material. These consist of: primary radicals ($R^{\bullet}$), macroradicals ($M^{\bullet}$), monomer (M), polymer (P), and an inhibitor (Z).

Previously, [7, 10, 11, 16, 18], it was assumed that the effect of inhibition during exposure was due solely to the initially dissolved oxygen present within the photopolymer layer. However, when the photopolymer is exposed to a sinusoidal interference pattern, the initial concentration of dissolved inhibiting oxygen reacts with the primary radicals produced in the bright illuminated regions. This non-uniform irradiance of the exposing intensity pattern, see Fig. 1, causes inhibitor concentration gradients, and hence a diffusion of oxygen from the dark unexposed regions to the bright exposed regions occurs. As the relative size of oxygen molecules is small compared to the surrounding material components, it can be assumed that the oxygen is relatively free to diffuse rapidly [17], resulting in a one-dimensional standard diffusion equation for the concentration of inhibitor which can be represented by,

$$\frac{\mathrm{d}Z(x,t)}{\mathrm{d}t} = \frac{\mathrm{d}}{\mathrm{d}x}\left[D_z\frac{\mathrm{d}Z(x,t)}{\mathrm{d}x}\right] - k_{z,R^{\bullet}}Z(x,t)R^{\bullet}(x,t) - k_{z,M^{\bullet}}Z(x,t)M^{\bullet}(x,t), \tag{8}$$

where Z is the instantaneous inhibiting oxygen concentration and D_z is the diffusion constant of oxygen in the dry material layer, which in this analysis will be assumed to be time and space independent. The inhibition rate constants, $k_{z,R^{\bullet}}$ and $k_{z,M^{\bullet}}$, in the reactions presented in Eqs. 5a and 5b, will in general have different values (of reactivity) due to the differences in their relative molecular sizes, [10], however in this analysis, for the sake of simplicity they will be treated as being equal, i.e., $k_z = k_{z,R^{\bullet}} = k_{z,M^{\bullet}}$. The initial condition for this diffusion equation is $Z(x,0) = Z_0$, for $-\infty < x < \infty$, where Z_0 is the initial concentration of dissolved oxygen which can be measured using a dissolved oxygen probe.

Analyzing the photochemical reactions for the generation and removal of primary radicals yields the governing equation of its concentration in time and space,

$$\frac{\mathrm{d}R^{\bullet}(x,t)}{\mathrm{d}t} = R_i(x,t) - k_i R^{\bullet}(x,t)u(x,t) - k_{\mathrm{tp}}R^{\bullet}(x,t)M^{\bullet}(x,t) - k_z R^{\bullet}(x,t)Z(x,t), \tag{9}$$

where $u(x,t)$ is the free-monomer concentration, (denoted earlier by M). This equation states that the rate of change of primary radical concentration is equal to the amount of primary radicals generated by photon absorption, Eq. 6, minus the amounts removed by: (a) the initiation of macroradicals; (b) primary termination with growing polymer chains; and (c) inhibition by oxygen, see Eqs. 2b, 4c, and 5a, respectively.

Including both types of termination mechanism (primary and bimolecular) and the effects of inhibition, the equation governing macroradical concentration is

$$\frac{\mathrm{d}M^{\bullet}(x,t)}{\mathrm{d}t} = k_{\mathrm{i}}R^{\bullet}(x,t)u(x,t) - 2k_{\mathrm{t}}[M^{\bullet}(x,t)]^2 - k_{\mathrm{tp}}R^{\bullet}(x,t)M^{\bullet}(x,t) - k_z Z(x,t)M^{\bullet}(x,t), \tag{10}$$

where the squared term represents the effect of bimolecular termination. The generation term in this equation appears as the removal term due to macroradical initiation in Eq. 9.

When the layer is exposed to the interference pattern, monomer reacts with the primary radicals produced by photon absorption. The non-uniform irradiance creates monomer concentration gradients as discussed earlier, and as a result monomer diffuses from the dark regions to the monomer depleted exposed regions. This enables us to represent the monomer concentration using the following one-dimensional diffusion equation,

$$\frac{\mathrm{d}u(x,t)}{\mathrm{d}t} = \frac{\mathrm{d}}{\mathrm{d}x}\left[D_{\mathrm{m}}(x,t)\frac{\mathrm{d}u(x,t)}{\mathrm{d}x}\right] - k_{\mathrm{i}}R^{\bullet}(x,t)u(x,t) - \int_{-\infty}^{\infty} G(x,x')F(x',t)u(x',t)\mathrm{d}x', \tag{11}$$

where $F(x,t)$ is the polymerization rate and $D_{\mathrm{m}}(x,\ t)$ represents the monomer diffusion constant, [6–8, 12, 21]. $G(x,x')$ is the non-local material spatial response function:

$$G(x,x') = \frac{1}{\sqrt{2\pi\sigma}} \exp\left[\frac{-(x-x')^2}{2\sigma}\right], \quad (12)$$

where σ is the constant non-local response parameter normalized with respect to the distance between consecutive bright fringes (period), Λ, [6–8, 12]. This non-local response function represents the effect of initiation at location x' on the amount of monomer polymerized at location x, [6–8, 12]. The initial monomer concentration for $-\infty < x < \infty$ is $u(x,0) = U_0$ (mol/cm^3).

In previous theoretical models, which were based upon the steady state approximation presented in Eq. 1, there is a square root dependence of polymerization rate on the rate of initiation. Therefore in order to fully remove the steady state assumption it is necessary to suitably adjust the representation for the polymerization rate, so that it is expressed as a function of the solution to the non-steady state equation for monomer radical concentration, Eq. 10. In this case we obtain

$$F(x,t) = k_p M^\bullet(x,t), \quad (13)$$

where k_p is the propagation rate. The spatial distribution of the polymerization rate is accounted for by the generation/production of primary radicals in the areas exposed by the co-sinusoidal irradiance, Eq. 6.

The concentration of polymerized monomers after an exposure of duration t is given by

$$N(x,t) = \int_0^t \int_{-\infty}^{+\infty} G(x-x')F(x',t')u(x',t')\mathrm{d}x'\mathrm{d}t', \quad (14)$$

where N represents the concentration of polymerized monomer.

As the generation of both the primary radicals, monomer radicals, polymer and the removal of monomer and inhibiting oxygen are dependent upon the spatial distribution of exposure irradiance; their concentrations will also be periodic even functions of x. Thus, the expressions in Eqs. 8–11, can all be written as Fourier series

$$X(x,t) = \sum_{j=0}^{\infty} X_j(t)\cos(jKx), \quad (15)$$

where X represents $R^\bullet$, $M^\bullet$, u, Z, N, and D_m. A set of first order coupled differential equations can then be obtained by gathering the coefficients of the various co-sinusoidal spatial contributions and writing the equations in terms of these time varying spatial harmonic amplitudes. Assuming that harmonics of order greater than $j = 3$ are negligible, we obtain sets of first-order coupled differential equations, which must be solved with the following initial conditions, $Z_0(t=0) = Z_0$, $u_0(t=0) = U_0$, $A_0(t=0) = A_0$, $u_{n>0}(t=0) = R^\bullet_{n>0}(t=0) = 0$, and $M^\bullet_{n>0}(t=0) = N_{n>0}(t=0) = 0$.

Experimental examination

Material composition and preparation

A typical photopolymer material consists of a photosensitizer, an electron donor, a monomer, a cross-linker, and a binder. They can be made sensitive to a particular wavelength by using a particular photosensitive dye. In this study the chosen photosensitiser used is Erythrosin B, therefore holographic recording was carried out using a green Solid-State Crystal Laser of wavelength, $\lambda = 532$ nm.

Our standard AA/PVA material was made using the components listed in Table 1 with the exclusion of the chain transfer agent, Sodium Formate, HCOONa. The material can be prepared as follows:

(a) Ten gram of PVA (binder) was added to 100 cm^3 of deionized water and dissolved using a heater/stirrer. This solution is then allowed to cool and 70 cm^3 of this solution is transferred into a beaker.
(b) A total of 8 cm^3 of Triethanolamine (electron donor) was added to the PVA solution and stirred thoroughly.
(c) A total of 2.4 g of Acrlyamide (monomer) and 0.8 g of Bis-acrylamide (cross linker) were added to the PVA solution under a fume cupboard and stirred until completely dissolved. In order to include the chain transfer agent into the standard material composition,

Table 1 Components and volume fractions of the material make up

Component	Function	Mass (g)	Density (g/cm^3)	Volume (cm^3)	Standard volume fraction	Volume fraction with CTA
PVA	Binder	7	1.3	5.384615	0.333025	0.32797
AA	Monomer	2.4	1.122	2.139037	0.132294	0.13028
BA	Cross-linker	0.8	1.24	0.645161	0.039902	0.03929
TEA	Donor	8.992	1.124	8	0.49478	0.48727
HCOONa	CTA	0.48	1.92	0.25	0	0.01522

0.48 g of Sodium Formate would be added to the mixture at this point.

(d) A total of 16 cm^3 of 2×10^{-4} M Erythrosin B (photosensitizer) is added to the beaker. This step and subsequent steps were carried out under a safety light, as the material is now sensitive to green light.

(e) The solution is then made up to 100 cm^3 in a volumetric flask with de-ionized water.

(f) The solution is then stored in the dark ready for plate preparation.

To prepare dry material layers for holographic recording the solution prepared above is used as follows:

(1) The glass substrates are placed on a level surface so that the photopolymer layers would adhere to the glass evenly, producing a layer of uniform thickness.

(2) A total of 2 cm^3 of the photopolymer solution is then deposited evenly over the area of the glass plate using a syringe drop casting.

(3) Using this method the typical material thickness is 100 ± 10 μm. Different thicknesses can be obtained by depositing different quantities of material. The thickness and uniformity of these layers can be measured using a micrometer screw gauge or using transmission theory.

(4) The plates are then left in the dark for approximately 24 h until dry. Drying times are dependent on the thickness of the material and the relative humidity.

(5) Once dried the plates are stored in a lightproof desiccator ready for use.

Holographic setup and testing

In the study of holographic recording materials it is common to record gratings in photosensitive materials, such as photopolymers, and to then optically examine the resulting grating formation, see Fig. 4. The gratings produced are often modelled using Kogelnik's two-wave coupled wave theory, [22], which describes the efficiency with which thick (volume) holograms can diffract incident light, I_{in}. Analytic expressions for both the angular and wavelength dependence of the diffraction efficiency, $\eta(t)$ as the incident light deviates from the Bragg condition are derived. Thus the dependence of the diffraction efficiency, $\eta(t) = I_D(t)/I_{in}$, where I_{in} and $I_D(t)$ are the incident and diffracted probe beam intensities, respectively (see Fig. 4), on a number of grating parameters is known. For a lossless, unslanted volume transmission geometry grating, replayed on-Bragg with TE polarized probe light, an expression for the time variation of the refractive index modulation can be obtained,

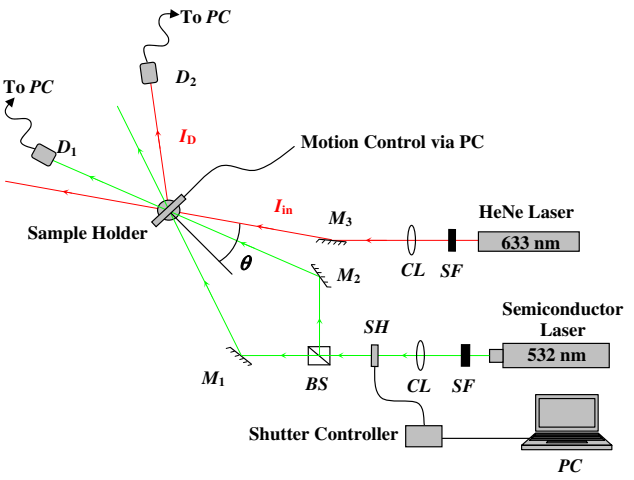

Fig. 4 Typical experimental set-up used to record unslanted volume transmission holographic gratings with a recording wavelength of $\lambda = 532$ nm. *CL* collimating lens, *SH* electronic shutter, *SF* spatial filter, D_1 and D_2 power meter detectors, *BS* beam splitter, M_1, M_2, and M_3 mirrors

$$n_1(t) = \frac{\lambda \cos\theta}{\pi d} \sin^{-1}\left[\sqrt{\frac{I_D(t)}{I_{in}}}\right], \tag{16}$$

where d represents the material layer thickness, θ and λ are the Bragg angle and wavelength of incident probe beam inside the grating. In deriving Eq. 1 all boundary reflections have been neglected. As discussed earlier in "Introduction" section, the refractive index modulation $n_1(t)$ can be assumed to be proportional to the amount of polymer generated. This relationship can be represented by the expression, $n_1(t) = C_p N_1(t)$, where C_p is a constant of proportionality and $N_1(t)$ is the first harmonic of polymer concentration, see Eq. 14, [7, 23]. Therefore, monitoring the intensity of the resulting probe diffracted beam, $I_D(t)$, and thus the diffraction efficiency, enables the calculation of the strength of the grating, i.e., the refractive index modulation, n_1. Therefore, it is possible to monitor the grating formation (growth curve) by recording the intensity of the diffracted beam, $I_D(t)$, as suggested by Eq. 16. From this, knowledge about the temporal evolution of the polymer concentration is known and therefore using the photochemical model developed in "Model development" section, information about the relative rates of reactions, of the other species within the material can be obtained, i.e., $R_i(x,t)$, $F(x,t)$, etc.

One of the main advantages of many photopolymer materials is that they are self-processing and thus, non-latent, therefore the diffractive scattering properties are immediately available as the grating is being formed. This allows the evolution of the grating to be monitored by replaying the grating as it is being recorded using a probe

laser with a wavelength, which lies outside the absorption spectrum of the photosensitizer used. This ensures that probing does not affect the fabrication process. In the set-up presented in Fig. 4 the probe laser is a HeNe laser operating at $\lambda = 633$ nm, i.e., outside the absorption spectrum of the photosensitizer, Erythrosin B.

Model predictions

The predictions of the model presented in "Model development" section are now discussed. Numerical results describing the behavior of the monomer and polymer concentrations are examined, and $n_1(t)$ is then calculated using the relation, $n_1(t) = C_p N_1(t)$. Comparisons of the results of simulations performed retaining 4, 8, and 12 concentration harmonics are made in order to assess the numerical convergence of retaining higher harmonics of the Fourier Series expansion, see Eq. 15.

Since all the simulations presented in this section are generated assuming the same exposure intensity and material thickness, the values used to predict the time variation in absorbed intensity, Eq. 7 are as follows; $\varepsilon = 2 \times 10^8$ cm^2/mol, $\phi = 0.021$ mol/Einstein, and $T_{sf} = 0.74$. $\Phi = 0.2$, is the number of radicals produced per photon absorbed, Eq. 6. These values appear in the literature, [16, 19], and were estimated from fits to standard AA/PVA experimentally data. The coupled differential equations derived and presented in "Model development" section, are then solved using the aforementioned initial conditions, where $U_0 = 2.83 \times 10^{-3}$ mol/cm^3 and $Z_0 = 1 \times 10^{-7}$ mol/cm^3. The other parameters used are as follows: $k_p = 1.6 \times 10^6$ cm^3 mol^{-1} s^{-1}, $k_t = 9 \times 10^7$ cm^3 mol^{-1} s^{-1}, $k_{tp} = 1 \times 10^{11}$ cm^3 mol^{-1} s^{-1}, $k_i = 5 \times 10^7$ cm^3 mol^{-1} s^{-1}, $D_m = 2 \times 10^{-11}$ cm^2 s^{-1}, $k_z = 5 \times 10^8$ cm^3 mol^{-1} s^{-1}, and $D_z = 5 \times 10^{-8}$ cm^2 s^{-1}. The spatial frequency assumed in these simulations is 1000 lines/mm, and the non-local response length chosen to be $\sqrt{\sigma'} = 54$ nm, [6–9, 12, 23].

Plots of the amplitudes of the first two harmonics of the monomer and polymer concentrations, as a function of time, are presented in Figs. 5 and 6, respectively. In both plots the *solid line* represents the solutions when 4 harmonic, i.e., $R_j^\bullet$, $M_j^\bullet$, and u_j for $0 < j < 4$, are retained during the numerical solution of the coupled differential equations, the *short dashed lines* represent the solutions generated with the retention of 8 harmonics, and the *long dashed lines* represent the solutions generated with 12 harmonics. In all cases two harmonic of the inhibitor concentration, i.e., Z_j for $0 < j < 2$, is retained.

As can be clearly seen in both figures there is good general agreement between the simulations generated using 4, 8, and 12 harmonics. For both the monomer and the polymer concentration harmonic amplitudes the differences between the 4 and 8 harmonic simulations, (2.5% max), are greater than those between the 8 and 12 harmonic simulations, (1% max). This suggests that the system is numerically stable and that the model converges rapidly with the inclusion of higher order harmonics.

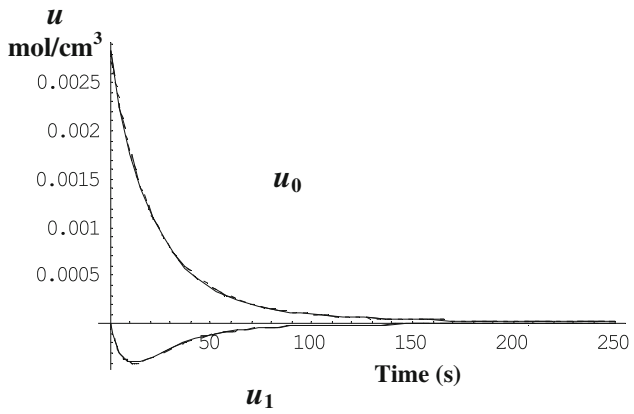

Fig. 5 Predictions of the amplitudes of the first two harmonics of monomer concentration, u_0 and u_1, when 4 (*solid line*), 8 (*short dashed line*), and 12 (*long dashed line*), harmonics are retained during the simulations

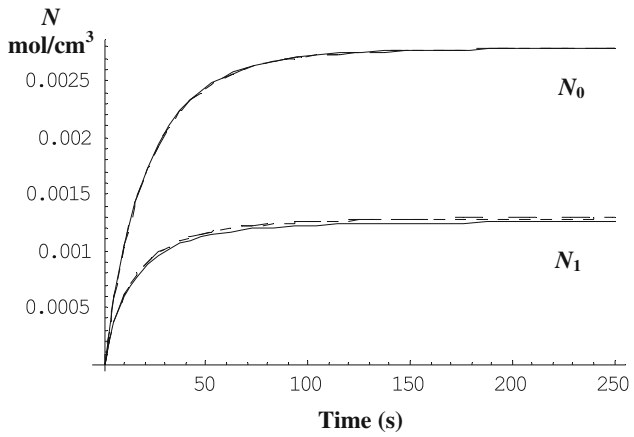

Fig. 6 The amplitudes of polymer concentration, N_0 and N_1, when 4 (*solid line*), 8 (*short dashed line*), and 12 (*long dashed line*), harmonics are retained

In order to simulate the temporal evolution of grating refractive index modulation for 4, 8, and 12 harmonics, as presented in Fig. 7, the proportionality constant was chosen to be $C_p = 1.44$ cm^3/mol. This proportionality constant is directly related to the average refractive index of the material and that of the individual refractive indices of the components within the material. Again it can be seen that there is good convergence with the retention of higher concentration harmonics.

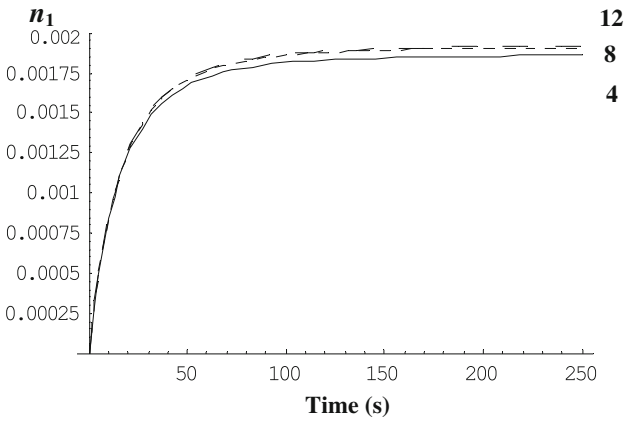

Fig. 7 Comparison of the simulated growth curves for the holographic grating refractive index modulation, for a 2 mW/cm^2 exposure, for 4 (*full line*), 8 (*short dashed line*), and 12 (*long dashed line*) harmonics

Results and discussion

We now examine the response of: (a) the standard AA/PVA photopolymer material; and (b) the AA/PVA photopolymer material with added sodium formate CTA, to different spatial variations in the exposing interference pattern (spatial frequencies), i.e., examining their ability to record high frequency information, (high resolution). We do this by comparing the growth curves and the saturation values of refractive index modulation for a range of spatial frequencies. For each spatial frequency examined, growth curves were recorded with an exposing intensity of 8 mW/cm^2, ($\lambda = 532$ nm) using the set-up described in Fig. 4. In all cases the diffraction efficiency of the probe beam ($\lambda = 633$ nm) was monitored during all of the exposure. An average growth curve, and appropriate error bars, were identified for each of the spatial frequencies and were then converted into grating refractive index modulations using Eq. 1, [22]. The NPDD model was then applied to calculate the first harmonic of polymer concentration $N_1(t)$.

The experimental growth curve data were then fit using the NPDD model predictions. A least squares algorithm, (in which the Mean Square Error (MSE) between the prediction and the experimental data is the cost function which is minimized), is used to obtain the best fit as a function of the material parameters values. In this way the monomer diffusion constant D_m, the propagation rate constant, k_p, the bimolecular termination rate constant, k_t, the refractive index proportionality constant C_p, and the non-local parameter, $\sqrt{\sigma'}$ were extracted. To simplify the exhaustive search, two assumptions were made: (i) the initiation rate constant, k_i, was assumed to be equal to the propagation rate constant, k_p; and (ii) the primary termination rate constant, k_{tp}, was assumed to be equal to the bimolecular termination rate constant, k_t.

The values $\varepsilon = 2 \times 10^8$ cm^2/mol, $\phi = 0.021$ mol/Einstein, and $T_{sf} = 0.74$ from "Reaction mechanisms" section are again used with the initial concentrations of photosensitizer and inhibitor, $A_0 = 1.034 \times 10^{-6}$ mol/cm^3, and $Z_0 = 1 \times 10^{-7}$ mol/cm^3 for material layers of thickness $d \approx 100\mu$m. The inhibition rate constant was chosen to be $k_z = 1.6 \times 10^9$ cm^3/mol-s.

The parameters estimated from fitting the NPDD model to the experimental growth curves for both materials are presented in Table 2. For each spatial frequency the saturation refractive index modulation value is given, $[n_1^{sat}]$, in the second column of each table. Examining the parameter estimates for k_p, k_t, and C_p from both tables, it can be seen that they are comparable to one another and to values in the literature [7, 23]. The values obtained for the diffusion constant D_m, lie within the search ranges and support the results obtained in our most recent work on diffusion in photopolymers [7]. For the standard AA/PVA material the mean non-local response length was estimated to be approximately $\sqrt{\sigma'} \approx 63$ nm. This value agrees with the previous estimates in the literature [6–8, 12, 23]. For AA/PVA with CTA, the corresponding value is $\sqrt{\sigma'} \approx 50$ nm. This corresponds to a $\sim$20%, reduction in the mean $\sqrt{\sigma'}$ value.

Examining the values of the other parameters extracted and presented in Table 2 several important points must be made. First, the quality of the numerical fits achieved in all cases is all comparably good, with typical MSE values of $\sim 10^{-10}$. Second following an exhaustive and independent

Table 2 Parameter extraction from fits to experimental data for: (a) Standard material (AA/PVA) with no chain transfer agent; and (b) Standard (AA/PVA) with chain transfer agent material

Material	SF (lines/mm) $[n_1^{sat} \times 10^{-3}]$	k_p ($\times 10^7$) cm^3/mols	k_t ($\times 10^{10}$) cm^3/mols	D_m ($\times 10^{-11}$) cm^2/s	C_p cm^3/mol	$\sqrt{\sigma'}$ (nm)	MSE ($\times 10^{-10}$)
NO CTA	1000 [1.81]	4.00	0.84	2.00	1.39	56	1.41
	2000 [1.01]	4.18	0.65	0.80	1.23	66	1.17
	2750 [0.42]	2.09	1.00	0.95	1.10	71	0.54
CTA	1000 [1.85]	4.00	1.14	1.90	1.44	55	1.32
	2000 [1.17]	4.00	0.60	0.62	1.30	50	1.46
	2750 [0.50]	3.01	1.20	1.10	1.11	55	1.22

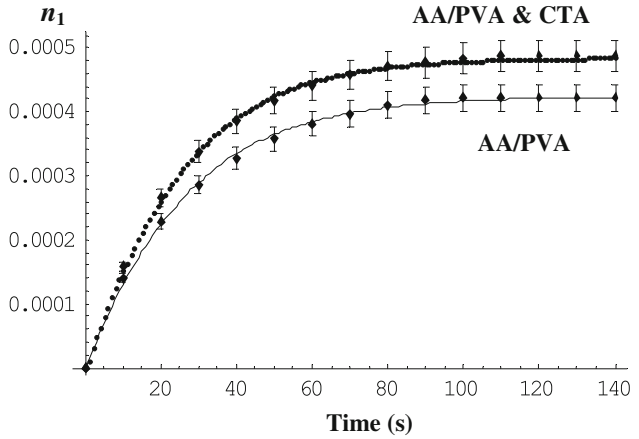

Fig. 8 Experimental growth curve data and fits at 2750 lines/mm spatial frequency where the standard material (*solid line*) and the standard material with the inclusion of chain transfer agent (*dashed line*)

search procedure the mean values of all the other parameters estimated remained similar while only the non-local parameter varied significantly.

To more clearly illustrate the improvement in material performance, and to demonstrate the quality of our numerical fits to the data, the results used to produce the row of parameter values, in Table 2, for the 2750 lines/mm spatial frequency case, are shown in Fig. 8. The data presented, and the associated error bars, result from 5 to 10 repetitions of the same exposure in identically produced and exposed dry layers. For this concentration and type of CTA an average improvement of $\sim$17% in the refractive index modulation is observed.

Conclusion

Following a detailed discussion of free radical photopolymerization, a kinetic model, which includes most of the major photochemical effects, which take place during holographic grating formation, has been presented. The model includes the effects of: (i) non-steady state kinetics; (ii) spatially and temporally non-local polymer chain growth; (iii) time varying photon absorption; (iv) multiple termination mechanisms; and (v) inhibition.

The spatial frequency response of an AA/PVA photopolymer has been improved through the addition of a chain transfer agent (CTA), sodium formate. This improvement has been confirmed through the estimation of material parameters using the extended NPDD model. The CTA has the effect of decreasing the average length of the PA chains formed, thus reducing the non-local parameter, from 63 nm to 50 nm. Given that a C–C bond is approximately 0.15 nm long and that a carbon atom is $\sim$0.1 nm long, a PA repeat unit of length 0.5 nm would not be unexpected. Given that coiled polymer chains may contain from hundreds to tens of thousands of repeat units, the lengths predicted by this model seem physically reasonable.

Acknowledgements We acknowledge the support of Enterprise Ireland, Science Foundation Ireland and the Irish Research Council for Science, Engineering and Technology.

References

1. Dahr L, Hale A, Kurtis K, Schnoes M, Tackitt M, Wilson W, Hill A, Schilling M, Katz H, Olsen A (2000) Photopolymer recording media for high density data storage. Conference Digest, Optical Data Storage. IEEE, NJ, pp 158–160
2. Schultz S, Glytsis E, Gaylord T (2000) Appl Opt 39:1223
3. Manivannan G, Lessard RA (1994) Trends Polym Sci 2:282
4. Syms RRA (1990) Practical volume holography. Clarendon Press, Oxford
5. Lawrence JR, O'Neill FT, Sheridan JT (2001) Optik 112(10):449
6. Kelly JV, Gleeson MR, Close CE, O'Neill FT, Sheridan JT, Gallego S, Neipp C (2006) J Appl Phys 99(11):113105
7. Gleeson MR, Sabol D, Liu S, Close CE, Kelly JV, Sheridan JT (2008) J Opt Soc Am B 25(3):396
8. Sheridan JT, Lawrence JR (2000) J Opt Soc Am A 17(6):1108
9. Gleeson MR, Sheridan JT (2009) J Opt A Pure Appl Opt 10:024008
10. Odian G (1991) Principles of polymerization. Wiley, New York
11. Gleeson MR, Kelly JV, Sabol D, Close CE, Liu S, Sheridan JT (2007) J Appl Phys 102(2):023108
12. Kelly JV, Gleeson MR, Close CE, O'Neill FT, Sheridan JT, Gallego S, Neipp C (2005) Opt Exp 13(18):6990
13. Bamford CH, Jenkins AD, Johnston R (1959) Trans Faraday Soc 55(8):1451
14. Goodner MD, Lee HR, Bowman CN (1997) Ind Eng Chem 36(4):1247
15. Goodner MD, Bowman CN (1999) Macromolecules 32(20):6552
16. Gleeson MR, Liu S, O'Duill S, Sheridan JT (2008) J Appl Phys 104(7):064917
17. O'Brien AK, Bowman CN (2006) Macromol Theory Simul 15(2):176
18. Gleeson MR, Kelly JV, Close CE, O'Neill FT, Sheridan JT (2006) J Opt Soc Am B 23(10):2079
19. Liu S, Gleeson MR, Sheridan JT (2009) J Opt Soc Am B 26(3):1
20. Manabe T, Utsumi T, Okamura S (1962) J Polym Sci 58(166): 121
21. Zhao GH, Mouroulis P (1994) J Mod Opt 41(10):1929
22. Kogelnik H (1969) Bell Syst Tech J 48(9):2909
23. Kelly JV, O'Neill FT, Sheridan JT, Neipp C, Gallego S, Ortuno M (2005) J Opt Soc Am B 22(2):407